CHARACTERIZING THREE DIMENSIONAL MICROSTRUCTURES FORMED BY PARTICLES: AN EXAMPLE OF ELECTROPHOTOGRAPHIC PRINTING TONER

Di Bai[a], Vineeth R. Patil[b], Marcos Esterman[c], and Shu Chang[a,b,*]

[a]College of Imaging Arts and Sciences
[b]College of Science
[c]Kate Gleason College of Engineering
[*]Corresponding Author
Rochester Institute of Technology, Rochester, NY 14623-5603

Abstract

Additive manufacturing of objects using powders can result in microscopic structures based on the properties of particles used. In additive manufacturing, piles of powder are consolidated by one or other mechanisms in order to form a part. The resulting microstructure within the part can impact its engineering performance. Predicting and controlling the engineering performance requires the characterization of the part's material interior microstructures. However, obtaining the microstructure is difficult since the interior of a powder is a challenge to visualize.

In this paper, unconsolidated powders are characterized. We have used Confocal Laser Scanning Microscopy to image three-dimensionally sediments of micron-sized poly-dispersed electro-photographic printing particles. Using image analysis tools, we have extracted each particle's position and radius in selected sampling volumes. Through this methodology, we demonstrate the possibility to recreate the three-dimensional particle structures and extract values for morphological parameters for powder systems. The feasibility of direct and quantitative particle structural characterization can lead to much needed methods and tools to relate particle structures to the process of fabrication, the design of materials, and product performance in additive manufacturing.

Introduction

Additive manufacturing technologies that use solid particles to construct parts share many similar issues with electrophotographic printing with solid toner. In both technologies, working with small individual particles gives a good flexibility in forming a part or an image from a bulk material. However, both techniques must comprehend how the individual particles will ultimately affect what is intended to be a continuous object. The particles will converge into an ensemble with certain morphology after deposition.

It is the particle morphology that determines the integrity of the ensemble and its material engineering performance. For example in the electrophotographic print (EP) process, the structure of the toner layer after deposition (the development stage) needs to be cohesive enough to successfully transfer from the

photoreceptor to paper under electrostatic fields and mechanical pressure without a significant change in structure to degrade the image quality. One would expect similar requirements for particle structures in the process of fabrication through additive manufacturing. The deposition of additional layers and the buildup of thermal energy can change the particle microstructure in a way that directly impact manufactured material quality. Creation of parts needs to meet certain engineering specifications, such as Young's modulus, and requires controllable microscopic structures for the powder. This microscopic structure depends not only on the particle material and size, but also on the particle delivery method.

The characterization of particle structures has been primarily conducted by extracting microstructural parameters from simulations and comparing simulations to experimental inferences [1]. With recent advancements in imaging technology and image analysis tools [2-5], there has been an intensified interest in directly imaging the powder particle microstructures and extracting quantitative metrics [2, 6, 7]. A number of studies have demonstrated the feasibility of more direct and quantitative characterizations of particle structures based on 3D imaging [2, 3]. As previous experiments have a successfully identified the particle positions and size, the next step is to use this information to determine the morphological parameters of structures.

It is the intention of this study to show the feasibility of quantifying powder morphology determined from 3D imaging. To demonstrate this feasibility, this initial study utilizes EP toner as the model material. EP materials have several advantages for this demonstration: (1) they fluoresce which enables the use of Confocal Laser Scanning Microscopy (CLSM), (2) the relationship between their particle morphology and print quality has been previously investigated [8, 9], and (3) there has been recent interests in the use of toner for additive manufacturing [10-15].

With CLSM and image analysis tools, we have obtained coordinates and radii for particles in selected sampling volumes, recreated the three-dimensional particle structures, and extracted values for several morphological parameters for this powder system. The feasibility of direct and quantitative particle structural characterization can lead to much needed methods and tools to relate particle structures to the process of fabrication, the design of materials, and product performance in additive manufacturing.

Background

1. Parameters for Particle Structures

The microstructure in a powder depends on the material properties of the particles it assembled from, such as the inter-particle cohesion, the particle size and distribution, the particle material composition, and the particle surface properties. Powder particles can form a wide range of microstructures. These particle microstructures can range from amorphous and compacted hard-sphere systems (such as soil, grain, etc.) [4, 5] to highly open structures with dendritic tentacles (such as printing particles [8, 9], dust particles in outer space) [16].

One parameter used frequently in describing a material's microstructure is the packing fraction, which is defined as the ratio of the total volume occupied by all the particles in a cell to the volume of the cell. For cohesive particles such as EP toner, the structure's packing fractions can be as low as 14% [8]. For large and non-cohesive particles such as grains, the structure's packing fraction can be close to the random close pack limit of around 58% [17]. Sands with different sizes and distributions have been observed with

a large porosity range. In a study by Al-Raoush *et al.*, 31% to 48% were measured for four different samples [5].

In addition to the packing fraction, other structural parameters include: (1) porosity, defined as the ratio of the empty space in the cell to the total volume of the cell, which is the supplement of the packing fraction; (2) local void ratio, defined as the ratio of the volume of the void space associated with the particle divided by the volume of the particle; and (3) coordination number, defined to be the average number of particles in contract with a given particle. Much of the part's structural parameters relate to the particles themselves through their materials properties, such as the inter-particle cohesion, particle sizes, and the particle size distribution.

The determination of structural parameters needs to be carried out with a large enough sample volume so that the parameters become independent on the size of the sample [5, 18-20]. This minimum sampling volume, which is named "representative elementary volume", [8, 9] signifies the scale of observation [5].

An additional terminology that characterizes the void regions is the concept of an "excluded region" or an "available space" in the representative elemental volume [21]. The "available space" is the empty space that additional particle or particles can be inserted; while the "excluded region" is the space where the existing deposited particles prevent the addition of an additional particle.

2. Correlations between Materials Performance and Particle Structures

Material macroscopic performances depend on the structural parameters [22-34]. For example, the work of Gao, *et al.*, indicates that the ductile fracture initiation toughness depends on the void volume fraction, the void shape, as well as the void distribution [23]. Gu *et al.* demonstrated that when energy density is insufficient, selectively laser-melted stainless steel will contain voids and untouched build particles in the material matrix produced [35]. The void region in amorphous (or random closed) particle packing has shown to be crucial to the behavior of particle systems [21]. Material properties have been observed as functions of the surface area and volume fraction of the available space [36]. For fluid flow through porous media, surfaces of the void region have been a subject of close investigation [37].

There are also numerous studies indicating the dependence of the object's performance on the properties of the particle from which it is composed. For instance, in the situation of amorphous packing, the packing density depends on the size distribution function [38]. In contrast, with cohesive particles, the packing density appears to be independent on particle sizes or the size distribution [8]. Frost [39] has reported that for two granular materials with the same void ratio, different preparation techniques could result in different mechanical responses. Chang *et al.* have shown that particles with similar compositions but different surface treatments could exhibit different packing and mechanical behaviors [9].

3. 3D Visualization

The ability to obtain particle positions in sample interiors through microscopic visualization is particularly appealing. The two main approaches have been Confocal Laser Scanning Microscopy (CLSM) and X-ray Computed Micro-Tomography (X-ray CMT).

Confocal Laser Scanning Microscopy (CLSM) is a high-resolution optical microscopy with depth selectivity and is capable of imaging interior structures for samples that are transparent and fluorescent. Much work has been conducted in colloidal solutions to take advantage of similar refractive indices

between particles and the fluid for optimal imaging [2, 6]. The methodology involves the capture of stacks (in the depth direction) of planar images and then the analysis of the image stacks through their pixelated values. It has been shown that the particle positions can be tracked and reconstructed into a 3D volume space [2, 3, 45]. The particles used in colloidal systems are typically monodispersed [2].

3D imaging with CLSM for micron-size particles in colloidal systems has contributed to substantial understanding on the atomic nucleation process and phase transitions [40-42]. Experimentations on these systems are performed with thin (a few layers of particles) and sometimes dilute samples for efficient light transmissions [43, 44]. The CLSM has also been employed for the studies of biological [42] systems. Included among the many CLSM applications for biological systems is the mapping of shape through the tracing of signals from fluorescence dyes that have been intentionally attached to the surface of the sampling objects. There is a lack of explorations of using CLSM for granular powders.

X-ray CMT has been used to study granular materials; primarily focusing on obtaining the representative distributions of local void ratios of porous media, evolution of the void ratio, localized deformations of granular materials [46, 47] and extraction of physically realistic pore network structure of porous media [48, 49]. Similar to CLSM, X-ray CMT captures stacks of images and performs analysis of images in pixelated values. Differently from CLSM, X-ray CMT does not require materials to be fluorescent. However, access to synchrotron radiation facility is needed in order to obtain high resolution imaging [50]. Much of studies of 3D particle mapping have been for much larger particles (~ mm scale) than are less interesting to additive manufacturing.

Due to the nature of print-based manufacturing, the product design and its material selections are intrinsically intertwined and cannot be separated. Well understood materials process-property-structure relationships can potentially lead to the establishment of a design framework that is unique to additive manufacturing. Although particle position tracking for colloidal and for millimeter-scale particle has been demonstrated, there is a lack of investigations for micron-size powder materials. This paper presents CLSM imaging of a model polydisperse micron-size powder material and the reduction of the structure it formed. In addition, this work reconstructs three-dimensionally the powder microstructures and extracts the powder system's structural parameters with quantifiable metrics.

3D Visualization and Particle Position Identification

1. Samples

Toner are typically 5-10 µm in diameters and consist of pigment (colorant), binders with both low and high melting point components, as well as charge- and flow-control agents (on the surface). All three colors, cyan, magenta, and yellow appear to fluoresce.

Yellow EP toner were used for this work and extracted from a HP3700 cartridge. The particle sediments were generated by dropping small quantities of toner onto a microscope glass slide using a spatula. Samples of sediments were enclosed with double-sided tapes and cover glasses on top to prevent toner contamination to the CLSM imaging system.

The sample deposition was not a well controllable process and resulted in variations in sample heights. Analysis volumes were determined by selecting regions with similar sample thicknesses.

2. Confocal Laser Scanning Microscopic Imaging

The CLSM imaging was conducted with a Leica TCS SP-5 Biological Confocal Microscope. The CLSM images were obtained with a 40X objective with Numerical Aperture of 1.1 and with water as the refractive medium to interface the objective lens and the sample cover glass slide. The sample was imaged in the fluorescence mode collected in the 475 nm – 610 nm range (with an excitation wavelength of 476 nm).

The images were collected at a lateral increment of approximately 0.05 μm x 0.05 μm and an increment of 0.17 μm in the depth direction. Cross-sectional images (XY plane of 44.5 μm x 44.5 μm, roughly the spot size deliverable by a 600 dots per inch digital document printer) were obtained in stacks as a function of depths (Z-axis).

The appearance of the "particle of interest" in the Z-position extends beyond the length of the radius measured in the XY plane. The prolate spheroid manifestation is caused by the three-dimensional diffraction pattern of light emitted from a small "point" source (toner in this case) [2, 51]. This effect is commonly observed and referred to as the actual image convoluted with a "point spread function" [2, 51]. The larger blurring in the Z direction gives the appearance of having more extent in that dimension. Although the effect causes elongation of the Z radii, the center position of the particle is not affected [51]. We assume these particles to be spherical based on observations of the particles in the XY plane. We have assigned the radius of each particle to be the maximum particle radius observed in the stack for that particle.
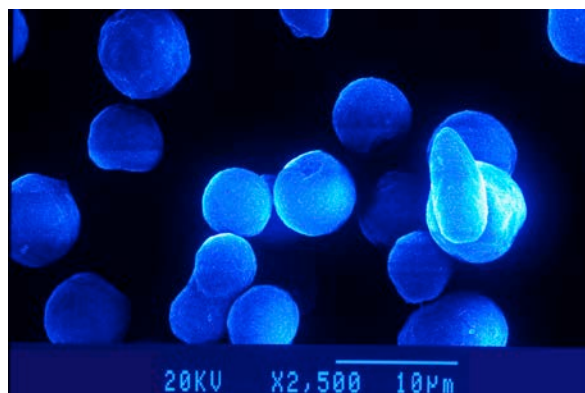

Figure 1. An SEM image of toner particles. Although most particles are approximately spheroids, there are particles taking on ellipsoidal shapes (A) as well as coalesced into agglomerates (B) (both encircled in the figure).

The Scanning Electron Microscopy (SEM) images were taken for the purpose to validate particle sizes and distribution. SEM was performed with a JEOL-JSM-6100 system on toner particles covered with Au prepared through evaporation. Figure 1 displays a sample SEM image of toner used to characterize the size distribution. Figure 1 shows that most toner particles are spheroids. However, there are a few that are more ellipsoidal in shape (such as the one encircled and labeled A). There also exist particles coalescing together to form agglomerates (such as the one encircled and labeled B). We excluded the ellipsoids and agglomerates from the size distribution estimation.

3. Deduction of Particle Positions and Radii from CLSM Images

Once a stack of cross-sectional images have been collected, each particle's (XYZ) coordinate and radius is identified through a four-step process: (1) select a particle to be the "particle of interest", (2) measure the (XY) coordinate and radius for the particle in each of the cross-sectional planes, (3) identify the maximum radius and the corresponding Z-plane where the maximum radius has occurred, and (4) select the Z value corresponding to the maximum radius plane to be the particle's Z-coordinate. The procedure was repeated for all particles in a selected sampling volume. Figures 2 and 3 illustrate this four-step process.

Figure 2 depicts (a) the top view of a sample and (b) a magnified region with one cross-sectional view. Fig. 2(a) shows that a 44.5 μm x 44.5 μm sampling specimens being boxed by a square in the upper left quandary of the image. This region is then selected for Z-stack imaging, as depicted with one view in fig. 2(b). Nine sampling specimens were examined.


44.5 μm x 44.5 μm imaging area
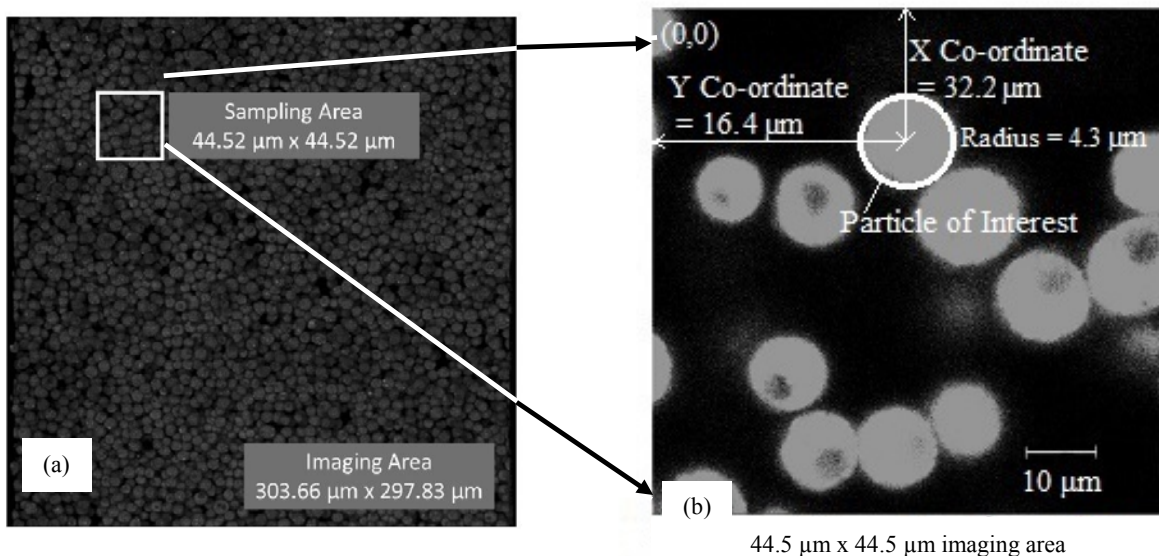
Figure 2. (a) Image of an area of toner from which a small boxed area marked by white lines is selected for sampling in the depth direction. (b) One cross-sectional image from the sampling area where a particle of interest is analyzed for its XY coordinate (32.2 μm, 16.4 μm) and radius (4.3 μm) with the origin of axes being at the top-left corner.

Fig. 2(b) displays a cross-sectional plane from the Z-stack of a "boxed" area. At this magnification, particles are visible and shown as grey areas (indicating fluorescence) through contrast against the black background (indicating no-fluorescence). The particles approximate spherical, with different diameters in appearance. Dark "cores" appearing inside of some of the particles shows the presence of a non-fluorescent material component within these particles. Conventional printing particles toners are known to incorporate more than one binder resins for the purpose of reducing the fixing/fusing temperature [52].

Also displayed in fig. 2(b) are the measured X coordinate, Y coordinate, and the radius for the "particle of interest" for a "particle of interest". This coordinate and radius determination is performed for all particles in fig. 2 (b) and for each of the cross-sectional image.

Figure 3 illustrates process to locate the Z-position for the "particle of interest". Displayed in fig. 3 are three cross-sectional images, (a), (b), and (c), corresponding to the same particle appearing in three different Z-planes. This particle is marked in all three images with identical circles (in white). The complete stack referenced fig. 3 measures 44.5 μm by 44.5 μm by 27.2 μm in dimension. The Z positions for the three cross-sectional planes in fig. 3 are 4.0 μm, 9.2 μm, and 13.0 μm for figures 3(a), 3(b) and 3(c) respectively, as measured with reference to the glass cover slide on top of the sediment.

As shown in fig. 3, with respect to the identical reference circle surrounding the particle, the particle appears in different sizes in three imaging planes as expected. Similarly, other particles also "appear" or "disappear" from each of the three views in fig. 3, as the cross sectional plane either intersects or does not intersect these particles.

44.5 μm x 44.5 μm
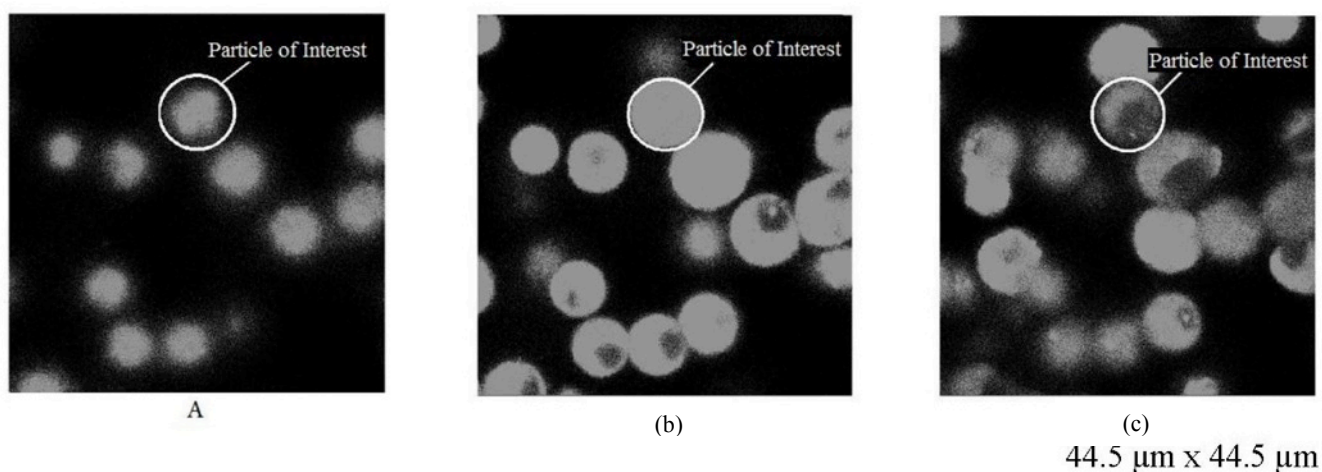
Figure 3. "Particle of interest" at three different image frames. The "particle of interest" is marked by the same sized circle in white. The figure shows: (a) appearance of fluorescence, b) emission at approximately full intensity, and c) diminishing of fluorescence. The largest radius of the particle occurs at around imaging frame (b). The imaging frame (b) provides the Z coordinate for the particle.

By comparison, the radius for the particle in 3(b) is greater that the radii in figs. 3(a) and 3(c). The radii measured from different planes for the particle are compared to find a maximal value. The Z position for the center of the particle is the Z-value for the maximal radius plane.

The Z positions for the particle centers are also attainable through the maxima of the fluorescence intensity profiles. However, this method is not chosen here because of the dark "cores" aforementioned which obscure the true maximum in the intensity profile. In addition, the particle displayed in the three cross-sectional images appears prolate in the Z direction. This is from the optical effect discussed in the section of Confocal Laser Scanning Microscopy Imaging. We have corrected this effect by using the radii obtained in the XY plane for the Z-direction for all particles.

Characterization of the Microstructure

Being able to extract coordinates and radii for the particles means that the individual particle parameters and the film's morphological parameters may be calculated quantitatively and directly.

1. Size Distribution
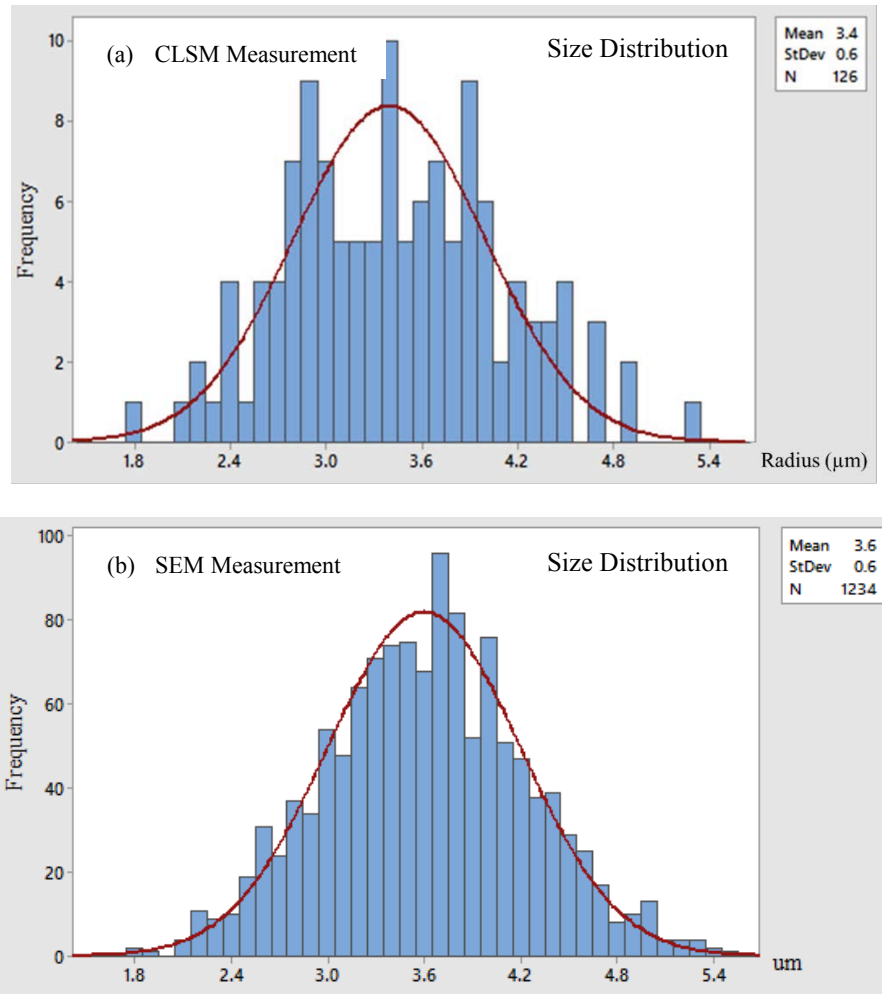
Figure 4. Size distributions attained from diameters measured from (a) CLSM and (b) SEM images respectively. SEM radii are slightly larger than those determined from CLSM images.

Figure 4 depicts the size distribution of toner particles with 4(a) measured from CLSM images and 4(b) measured from SEM images for the purpose of comparison and validation. With CLSM images, we evaluated 126 toner particles. Figure 4(a) shows that the particles have a normal distribution with a mean radius of 3.4 µm and a standard deviation of 0.6 µm. The particle sizes range from 1.8 µm to 5.4 µm. Figure 4(b) shows a similar distribution analyzed for an order of magnitude more particles. The mean radius obtained from SEM images is 3.6 µm with 0.6 µm as standard deviation. The larger particle size range signifies the polydispersive nature of toner.

Comparison between fig. 4(a) and 4(b) shows a slight difference in the mean radius as confirmed with a two-sample t-test. The smaller values from CLSM than those from SEM could be from diminishing fluorescence emissions at edges of the particles.

2. Particle Structure
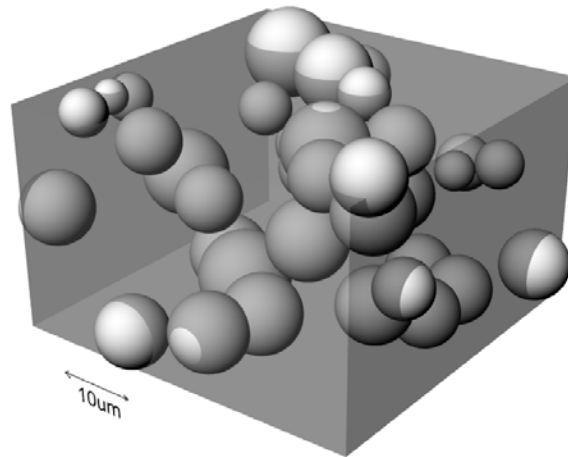
Figure 5. Reconstructed structure of toner particles in a volumetric unit of 44.5 µm x 44.5 µm x 27.2 µm. The "suspended" particles are in actual contacts with and being supported by particles in the neighboring volume cells. The structure is disorderly and open with much vacant space.
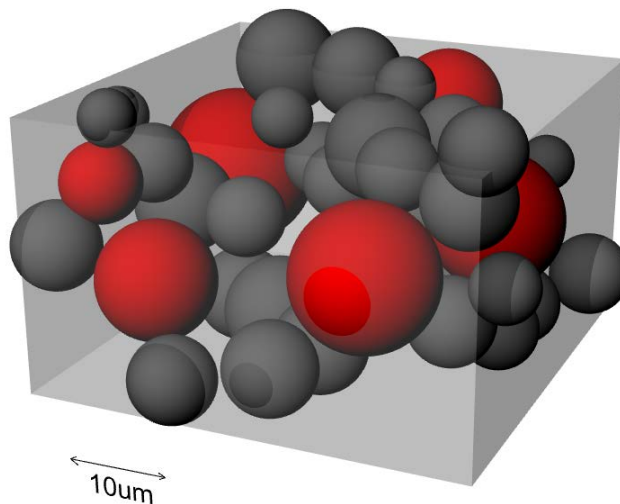
Figure 6. The same reconstruction as fig. 5; however, with red spheres inserted to illustrate spaces available for insertion of other materials.   I think this will rearrange once again when all the changes are accepted in the track changes feature

Using the XYZ coordinates and particle radii obtained, we are able to reconstruct the toner particle structures. An example of such a recreation is illustrated in fig. 5. The lighter portions of the spheres on

the outside of the reconstructed cell surfaces reflect the parts of particle volumes that do not contribute to the cell but are displayed here for visualization. The darker portions of the spheres represent the occupied space by the particles or the "excluded region". Figure 5 shows that some particles appearing "suspended" in space. These particles are in actual contact with and supported by particles in the neighboring cells.

Figure 6 exhibits the available space (in light grey) and the excluded particle volumes (in dark grey). For the purpose of illustration, the largest available volumes have been inserted with red particles to illustrate their possible dimensions. These vacant volumes represent regions that could potentially be used for material additions or become voids in the resulting material or product after post processing.

3. Particle Packing Fractions

In Figure 5, the particle cell reconstruction indicates very open structure and low particle packing fraction. The total volume occupied by the particles within the volumetric unit can be summed up from particles within the sampling cell and partial particles on the cell surfaces, edges and corners. This total volume of the particles within the cell, denoted V_p, can be calculated from:

$$V_p = \sum_i V_i(\text{interior}) + \sum_j V_j(\text{surfaces}) + \sum_k V_k(\text{edges}) + \sum_l V_l(\text{corners})$$

$$- \sum_m V_m(\text{particle double counted overlapping volumes})$$

(1)

Where i = number of particles in the interior, j = number of partial particles residing on the 6 surfaces and excluding those on the edges and at the corners, k = number of partial particles on the 12 edges and excluding those at the corners, l = number of partial particles at the 8 corners, and m = number of particles that overlapping the neighboring particles, all within a rectangular cube of w (width), h (height), and d (depth).

The packing fraction of the particle structure, denoted as Φ, is then:

$$\Phi = \frac{V_p}{V_c} = \frac{V_p}{w \times h \times d}$$

(2)

Theoretical simulations of Random Ballistic Deposition of cohesive particles predict a packing fraction of about 14.7% [8, 17]. Estimation from the particle measurement here has resulted in 13.3 ± 1.3 (%) packing fraction for the 9 samples examined. Comparable values between the result from this study and the predictions from simulations in the literature indicate that EP toners are cohesive with particle structures similar to that of the random ballistic deposition of cohesive particles.

4. Coordination Numbers

The reconstruction in fig. 5 reveals the tentacular nature of the structure formed by toner. Figure 7 contains one connected chain lifted from the particle cell depicted in fig. 5. Figs. 7(a) is the sphere representation and 7(b) presents the vectors connecting contacting spheres with the spheres reduced to solid dots. The example in fig. 7 indicates that particles in this chain have a coordination number between 1 and 3. In this example particle cell, there are four terminating particles with coordination number of 1, five particles each contacting two other particles, and two particles each with three contacting particles. This tentacle results in an average coordination number of 1.8.

(a)   (b)
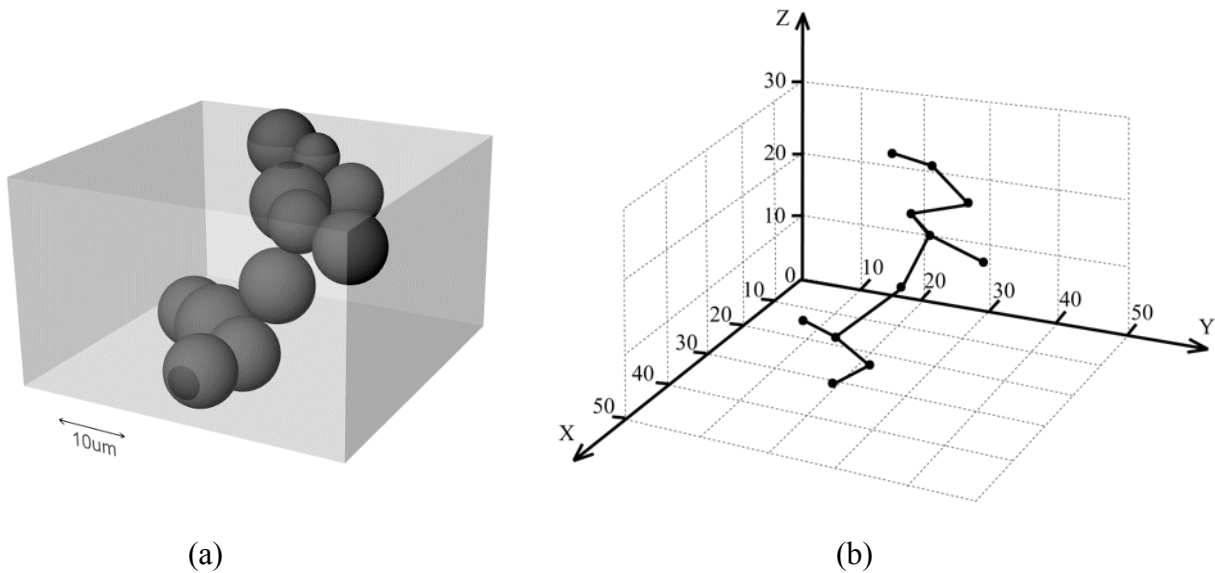
Figure 7. A connected chain has been lifted out from the cell reconstructed in fig. 5. Displayed in 7(a) is the chain and 7(b) is its stick-diagram for vectors connecting the particles. 7(b) shows most particles have two nearest neighbors.

The criterion to determine whether two particles are touching is the distance between the two particles being lesser than or equal to the sum of their radii. The coordination number illustrated with this particle chain is a characteristic of cohesive particles. In contrast, in the much studied random close packed sphere systems, the coordination number is approximately six per particle [53].

<u>Conclusion</u>

We have demonstrated the feasibility to determine particle positions in the interior of a powder, to visualize three-dimensionally the particle microstructure, and to quantitatively characterize the microstructure that the particles form. Using the Confocal Laser Scanning Microscopy and image analysis tools, we demonstrated this feasibility with EP toner in a sediment state. We have obtained and validated particle sizes and the particle size distribution observed through CLSM imaging. We have further employed this information to obtain the packing fraction of the toner system. In addition, we have

obtained examples of chain formations and the particle coordination numbers for a cohesive powder material.

Although Confocal Laser Scanning Microscope is limited to only fluorescent particle powders, X-ray CMT can potentially visualize non-fluorescent or metallic powders, with resolution depending on the X-ray sources. In such cases, similar analysis can be conducted to obtain the particle parameters for metallic and non-fluorescent powders.

The quantitative characterizations of the microscopic structures demonstrate direct measurement of particle structures. Such a measurement underscores a unique possibility to make significant progress in the understanding of the structure-property relationship for powder materials.

Acknowledgements

References

[1]   A. Hoffmann and H. Finkers, "A relation for the void fraction of randomly packed particle beds," *Powder Technology,* vol. 82, pp. 197-203, 1995.

[2]   M. C. Jenkins and S. U. Egelhaaf, "Confocal microscopy of colloidal particles: towards reliable, optimum coordinates," *Advances in Colloid and Interface Science,* vol. 136, pp. 65-92, 2008.

[3]   D. Semwogerere and E. R. Weeks, "Confocal microscopy," *Encyclopedia of Biomaterials and Biomedical Engineering,* pp. 1-10, 2005.

[4]   R. Al-Raoush and K. A. Alshibli, "Distribution of local void ratio in porous media systems from 3D X-ray microtomography images," *Physica A: Statistical Mechanics and its Applications,* vol. 361, pp. 441-456, 2006.

[5]   R. Al-Raoush and A. Papadopoulos, "Representative elementary volume analysis of porous media using X-ray computed tomography," *Powder Technology,* vol. 200, pp. 69-77, 2010.

[6]   W. C. Poon, E. R. Weeks, and C. P. Royall, "On measuring colloidal volume fractions," *Soft Matter,* vol. 8, pp. 21-30, 2012.

[7]   F. Brun, L. Mancini, P. Kasae, S. Favretto, D. Dreossi, and G. Tromba, "Pore3D: a software library for quantitative analysis of porous media," *Nuclear Instruments and Methods in Physics Research Section A: Accelerators, Spectrometers, Detectors and Associated Equipment,* vol. 615, pp. 326-332, 2010.

[8]   H. Mizes, "The structure of toner sediments simulated with random ballistic deposition," in *NIP 15: International Conference on Digital Printing Technologies*, pp. 495-498, Orlando, Florida, 1999.

[9] S. Chang, H. Till, E. Viturro, K. Watson, A. T. Perez, A. Gonzalez and A. Castellanos, "Measurement of toner cohesion in liquid inks using a visualization cell," in *NIP 14: International Conference on Digital Printing Technologies*, pp. 218-221, Toronto, Ontario, Canada, 1998.

[10] J. B. Jones, G. J. Gibbons, and D. I. Wimpenny, "Transfer methods toward additive manufacturing by electrophotography," in *NIP 27: International Conference on Digital Printing Technologies and Digital Fabrication 2011*, pp. 180-184, Minneapolis, Minnesota, 2011.

[11] A. V. Kumar and H. Zhang, "Electrophotographic powder deposition for freeform fabrication," in *10th Solid Freeform Fabrication Symposium*, University of Texas, Austin, Texas, 1999.

[12] D. Cormier, J. Taylor, and H. West, "An investigation of selective coloring with 3-D laser printing," *Journal of Manufacturing Processes,* vol. 4, pp. 148-152, 2002.

[13] A. V. Kumar and A. Dutta, "Electrophotographic layered manufacturing," *Journal of Manufacturing Science and Engineering,* vol. 126, pp. 571-576, 2004.

[14] A. K. Das, "An investigation on t he printing of metal and polymer powders using electrophotographic solid freeform fabrication," Doctoral dissertation, University of Florida, 2004.

[15] J. Jones, D. Wimpenny, G. Gibbons, and C. Sutcliffe, "Additive manufacturing by electrophotography: challenges and successes," in *NIP 26: International Conference on Digital Printing Technologies and Digital Fabrication 2010*, pp. 549-553, Austin, Texas, 2010.

[16] J. Blum and R. Schräpler, "Structure and mechanical properties of high-porosity macroscopic agglomerates formed by random ballistic deposition," *Physical Review Letters,* vol. 93, p. 115503, 2004.

[17] J. M. Valverde, and A. Castellanos, "Random loose packing of cohesive granular materials," *Europhysics Letters,* vol. 75, p. 985, 2006.

[18] S. Edwards and D. Grinev, "Compactivity and transmission of stress in granular materials," *Chaos: An Interdisciplinary Journal of Nonlinear Science,* vol. 9, pp. 551-558, 1999.

[19] T. Aste, M. Saadatfar, and T. Senden, "Geometrical structure of disordered sphere packings," *Physical Review E,* vol. 71, p. 061302, 2005.

[20] J. Bear and Y. Bachmat, "Introduction to modeling of transport phenomena in porous media*," Springer*, vol. 4, 1990.

[21] P. G. Debenedetti and T. M. Truskett, "The statistical geometry of voids in liquids," *Fluid Phase Equilibria,* vol. 158, pp. 549-556, 1999.

[22] A. S. Mayer and C. T. Miller, "The influence of porous medium characteristics and measurement scale on pore-scale distributions of residual nonaqueous-phase liquids," *Journal of Contaminant Hydrology,* vol. 11, pp. 189-213, 1992.

[23] X. Gao, T. Wang, and J. Kim, "On ductile fracture initiation toughness: effects of void volume fraction, void shape and void distribution," *International Journal of Solids and Structures,* vol. 42, pp. 5097-5117, 2005.

[24] H. Y. Sohn and C. Moreland, "The effect of particle size distribution on packing density," *The Canadian Journal of Chemical Engineering,* vol. 46, pp. 162-167, 1968.

[25] A. Dexter and D. Tanner, "Packing densities of mixtures of spheres with log-normal size distributions," *Nature,* vol. 238, pp. 31-32, 1972.

[26] R. Wakeman, "Packing densities of particles with log-normal size distributions," *Powder Technology,* vol. 11, pp. 297-299, 1975.

[27] G. Bierwagen and T. Sanders, "Studies of the effects of particle size distribution on the packing efficiency of particles," *Powder Technology,* vol. 10, pp. 111-119, 1974.

[28] N. Ouchiyama and T. Tanaka, "Porosity of a mass of solid particles having a range of sizes," *Industrial & Engineering Chemistry Fundamentals,* vol. 20, pp. 66-71, 1981.

[29] A. Yu and N. Standish, "A study of the packing of particles with a mixture size distribution," *Powder Technology,* vol. 76, pp. 113-124, 1993.

[30] G. G. Brown*,* A. S. Foust, D. L. V. Katz, "*Unit operations*," Wiley Publications, 1950.

[31] R. L. Flemmer, J. Pickett, and N. N. Clark, "An experimental study on the effect of particle shape on fluidization behavior," *Powder Technology,* vol. 77, pp. 123-133, 1993.

[32] E. F. o. C. Engineering and V. G. V. u. Chemieingenieurwesen, *"Particle characterization: 5th European symposium : preprints and abstracts,"* Nurnbergmesse, 1992.

[33] D. Geldart, "*Gas fluidization technology*," Wiley Publications, 1987.

[34] N. Harnby, A. Hawkins, and D. Vandame, "The use of bulk density determination as a means of typifying the flow characteristics of loosely compacted powders under conditions of variable relative humidity," *Chemical Engineering Science,* vol. 42, pp. 879-888, 1987.

[35] H. Gu, H. Gong, D. Pal, K. Rafi, T. Starr, and B. Stucker, "Influences of energy density on porosity and microstructure of selective laser melted 17-4PH stainless steel." *2013 Solid Freeform Fabrication Symposium,* pp. 474, 2013.

[36] S. Torquato, B. Lu, and J. Rubinstein, "Nearest-neighbor distribution functions in many-body systems," *Physical Review Letters A,* vol. 41, p. 2059, 1990.

[37] M. Sahimi, *"Flow and transport in porous media and fractured rock,"* Wiley Publications, 1995.

[38] H. AIKAWA*, et al.*, "Design for mutual separation of trace metals on the basis of HSAB rule," *Analytical Sciences,* vol. 7, p. 103, 1991.

[39] S. Sasloglou, J. Petrou, N. Kanellopoulos, and G. Androutsopoulos, "Realistic random sphere pack model for the prediction of relative permeability curves," *Microporous and Mesoporous Materials,* vol. 47, pp. 97-103, 2001.

[40] A. D. Dinsmore, E. R. Weeks, V. Prasad, A. C. Levitt, and D. A. Weitz, "Three-dimensional confocal microscopy of colloids," *Applied Optics,* vol. 40, pp. 4152-4159, 2001.

[41] V. Prasad, D. Semwogerere, and E. R. Weeks, "Confocal microscopy of colloids," *Journal of Physics: Condensed Matter,* vol. 19, p. 113102, 2007.

[42] J. B. Pawley and B. R. Masters, "Handbook of biological confocal microscopy," *International Society for Optics and Photonics, Third Edition,* vol. 13, 2008.

[43] C. P. Royall, W. C. K. Poon, and E. R. Weeks, "In search of colloidal hard spheres," *Soft Matter,* vol. 9, pp. 17-27, 2012.

[44] P. Schall, I. Cohen, D. A. Weitz, and F. Spaepen, "Visualization of dislocation dynamics in colloidal crystals," *Science,* vol. 305.5692, pp. 1944-1948, 2004.

[45] P. Habdas and E. R Weeks, "Video microscopy of colloidal suspensions and colloidal crystals," *Current Opinion in Colloid & Interface Science,* vol. 7, pp. 196-203, 2002.

[46] J. Desrues, R. Chambon, M. Mokni, and F. Mazerolle, "Void ratio evolution inside shear bands in triaxial sand specimens studied by computed tomography," *Géotechnique,* vol. 46, pp. 529 -546, 1996.

[47] K. A. Alshibli*, et al.*, "Assessment of localized deformations in sand using X-ray computed tomography," *ASTM Geotechnical Testing Journal,* vol. 23, pp. 274-299, 2000.

[48] R. Al-Raoush, K. Thompson, and C. S. Willson, "Comparison of network generation techniques for unconsolidated porous media," *Soil Science Society of America Journal,* vol. 67, pp. 1687-1700, 2003.

[49] R. Al-Raoush and C. Willson, "Extraction of physically realistic pore network properties from three-dimensional synchrotron X-ray microtomography images of unconsolidated porous media systems," *Journal of Hydrology,* vol. 300, pp. 44-64, 2005.

[50] L. Babout, "X-ray tomography imaging: a necessary tool for materials science," *Automatyka/Akademia Górniczo-Hutnicza im. Stanisława Staszica w Krakowie,* vol. 10, pp. 117-124, 2006.

[51] R. W. Cole, T. Jinadasa, and C. M. Brown, "Measuring and interpreting point spread functions to determine confocal microscope resolution and ensure quality control," *Nature Protocols,* vol. 6, pp. 1929-1941, 2011.

[52] S. Matsunaga, M. Ohno, T. Onuma, and M. Shimojo, "Toner with wax component for developing electrostatic image," *US Patent US5605778A*, 1997.

[53] E. Bromley and I. Hopkinson, "Confocal microscopy of a dense particle system," *Journal of Colloid and Interface Science,* vol. 245, pp. 75-80, 2002.